Electron detachment from negative ions in a short laser pulse

S. F. C. Shearer,* M. C. Smyth, and G. F. Gribakin†
School of Mathematics and Physics, Queen's University Belfast, Belfast, BT7 1NN, United Kingdom
(Received 23 May 2011; published 12 September 2011)

We present an efficient and accurate method to study electron detachment from negative ions by a few-cycle linearly polarized laser pulse. The adiabatic saddle-point method of Gribakin and Kuchiev [Phys. Rev. A **55**, 3760 (1997)] is adapted to calculate the transition amplitude for a short laser pulse. Its application to a pulse with N optical cycles produces $2(N+1)$ saddle points in complex time, which form a characteristic "smile." Numerical calculations are performed for H^- in a 5-cycle pulse with frequency 0.0043 a.u. and intensities of 10^{10}, 5×10^{10}, and 10^{11} W/cm^2, and for various carrier-envelope phases. We determine the spectrum of the photoelectrons as a function of both energy and emission angle, as well as the angle-integrated energy spectra and total detachment probabilities. Our calculations show that the dominant contribution to the transition amplitude is given by 5–6 central saddle points, which correspond to the strongest part of the pulse. We examine the dependence of the photoelectron angular distributions on the carrier-envelope phase and show that measuring such distributions can provide a way of determining this phase.

DOI: 10.1103/PhysRevA.84.033409 PACS number(s): 32.80.Rm, 32.80.Gc

I. INTRODUCTION

Rapid advances in experimental design in recent years have made it possible to study strong-field ionization by few-cycle laser pulses (see Ref. [1] and references therein). As a consequence of these huge technological advances in ultrafast laser technology, it has become possible to investigate physical processes at ever-smaller time scales. This has resulted in a shift in focus away from exploring strong-field ionization with long (i.e., many-cycle, periodic) pulses. The emphasis is now on addressing new theoretical challenges posed by unravelling the dynamics of strong-field ionization with few-cycle laser pulses. This dynamics is of fundamental interest for attosecond physics and related fields of science.

In this paper, we generalize the approach of Gribakin and Kuchiev [2] (GK) to describe multiphoton detachment of electrons from atomic negative ions in a short linearly polarized laser pulse. In particular, we explore the positions of the transition points in complex time on the parameters of the pulse and photoelectron momentum. We also investigate the influence of the phase shift between the pulse envelope and its carrier oscillation and show that the photoelectron angular distributions provide a reliable method for determining this phase.

The original theory of GK was based on the Keldysh approximation [3] and was developed to describe electron detachment from negative ions in a periodic laser pulse. In this approach, the quantum mechanical amplitude of transition of a bound electron into the final Volkov state is evaluated using the saddle-point method. It is given analytically by the contributions from two complex moments of time per period. One of the main results of GK was a demonstration that a proper application of the Keldysh approach to the photodetachment problem provides reliable quantitative predictions for the total rates and photoelectron energy spectra and angular distributions. It was also argued that the electron interaction with the laser field should be treated using the length gauge. The latter emphasizes large electron-atom separations, where the asymptotic form of the bound-state wave function can be used. The theory of GK is now widely used by other researchers in the field. It was extended by Kuchiev and Ostrovsky [4] to consider electron detachment in a bichromatic laser field. Reichle *et al.* [5] verified experimentally that the theory of GK successfully accounts for the predicted effect of quantum interference of electron trajectories in energy-resolved angular distributions for the negative hydrogen ion. Further experimental support of this approach was provided by a study of photodetachment of F^- in a strong linearly polarized pulse [6]. This work showed that GK was qualitatively able to reproduce the energy- and angle-resolved spectrum without needing to incorporate the rescattering mechanism, over the energy range studied.

Recently, there has been some disagreement in the literature over whether the length or velocity gauge is best adopted within the Keldysh-type theories [7,8]. However, it has been demonstrated experimentally by Bergues *et al.* [9] that the length gauge should be used in the description of the electron interaction with the laser field. This paper showed that the velocity gauge predicts a different interference structure in the electron energy and angular distributions compared with the length gauge. Direct comparison of the measurements with the length-gauge theory of [2] and the velocity gauge theory of [7] demonstrated that only the length-gauge approach within the strong-field approximation correctly reproduces the experimental data. Previous studies in the literature also showed that when only the leading order of the transition amplitude is retained, the model using the length gauge gives a more accurate description of strong-field ionization [10,11].

Experimental developments over the past decade have stimulated great interest in studying strong-field ionization by few-cycle laser pulses. In particular, the applicability of the saddle-point approach to short pulses was investigated in Ref. [12]. Subsequently, Martiny and Madsen [13] considered the photodetachment of atomic hydrogen and examined the effect of ellipticity of the laser pulse on the validity of

*f.shearer@qub.ac.uk
†g.gribakin@qub.ac.uk

the saddle-point method. They calculated the momentum distributions for using the Keldysh theory and compared their results with the saddle-point method. Their work showed that the saddle-point method is quite accurate in the linearly polarized case but gradually fails when the ellipticity is changed toward the circular case.

Arendt *et al.* [14] have studied electron detachment from negative ions by few-cycle laser pulses. In this work, they examined the occurrence of a nonmonotonic dependence of detachment probability on pulse duration. They showed that the results of their full numerical solution of the time-dependent Schrödinger equation compare favorably with the strong field approximation for weak and intermediate field strengths. However, for strong fields their results indicate that the strong-field approximation overestimates the exact numerical result. They also analyze momentum distributions where a nonmonotonic dependence of detachment probability on pulse duration occurs and show that a transition from a symmetric to an asymmetric momentum distribution evolves as the pulse duration is increased.

Another recent study on electron detachment from negative ions by ultrashort half-cycle electric-field pulses has been investigated [15]. In this work, the zero-range-potential model was used to calculate closed form expressions for momentum and energy distributions as well as for differential and integral detachment probabilities for a variety of pulse strengths and time delays between the action of one or two alternating "half-cycle pulses." The outcome of this research illustrated that the quantum interference of the wave packets formed during the interaction with each of the pulses can be fully accounted for by studying the momentum and energy distributions of the detached electrons. However, the authors noted that these effects were smoothed out in the energy, angular, and total detachment probabilities.

The aim of the present paper is to apply the formalism of Ref. [2] to short pulses and investigate in detail the behavior of the saddle points and the dependence of the total detachment probabilities, electron angular and energy distributions on the carrier-envelope phase (CEP) (cf. similar effects in double ionization [16]). We also investigate which saddle points give significant contributions to the transition amplitude. This analysis allows one to quantify to what extent the ionization by a short pulse is restricted to the times near center of the pulse where the electric field is strongest. In particular, we examine the spectrum of the photoelectrons as a function of both energy and emission angle and show that for a 5-cycle pulse the contributions of the 5–9 central saddle points gives the dominant contribution to examine the spectrum. We also calculate angle-integrated energy spectra and total detachment probabilities and consider the effect of varying the CEP on these quantites. Numerical calculations are performed for the negative hydrogen ion at three different peak intensities (10^{10}, 5×10^{10}, and 10^{11} W/cm^2) of the 5-cycle 10.6-μm laser pulse.

Section II below presents the basic equations of the Keldysh-saddle-point approach to the multiphoton electron detachment of negative ions in a short laser pulse. Section III shows the results of our numerical calculations and their analysis, with conclusions given in Sec. IV. Atomic units are used throughout, unless otherwise stated.

II. THEORY

A. Detachment amplitude and probability

Consider the detachment of a valence electron from an atom or negative ion in a short laser pulse. The electric field of the pulse with a sine-squared envelope may be defined as

$$\mathbf{F}(t) = -\frac{d\mathbf{A}}{dt}, \tag{1}$$

where

$$\mathbf{A}(t) = \frac{\mathbf{F}}{\omega}\sin^2\left(\frac{\omega t}{2N}\right)\sin(\omega t+\alpha). \tag{2}$$

Here, N is the number of optical cycles, ω is the frequency of the laser pulse, and α is the carrier-envelope phase. The photoelectron spectrum for a short pulse is determined by the differential detachment probability:

$$dw = |A_{\mathbf{p}}|^2\frac{d^3p}{(2\pi)^3}. \tag{3}$$

The amplitude $A_{\mathbf{p}}$ of electron ejection with momentum $\mathbf{p}$ is

$$A_{\mathbf{p}} = \int_0^\tau\int \Psi_{\mathbf{p}}^* V_F(t)\Psi_0 d\mathbf{r}dt, \tag{4}$$

where $\tau = 2\pi N/\omega$ is the duration of the laser pulse, Ψ_0 and $\Psi_{\mathbf{p}}$ are the wave functions of the initial and final states, respectively, and $V_F(t)$ is the interaction with the laser pulse. Note that the amplitude is different from that of Ref. [2]. The integral in Eq. (4) is over the whole pulse duration while the amplitude integral for the periodic pulse in Ref. [2] is over one period. Accordingly, Eq. (3) describes the detachment probability, as opposed to the detachment rate in the case of the long laser pulse.

The wave function $\Psi_0(\mathbf{r},t) = e^{-iE_0t}\Phi_0(\mathbf{r})$ describes an electron with energy $E_0<0$ bound in the atomic potential $U(\mathbf{r})$, where $\Phi_0(\mathbf{r})$ satisfies the Schrödinger equation:

$$\left[-\frac{\nabla^2}{2}+U(\mathbf{r})\right]\Phi_0(\mathbf{r}) = E_0\Phi_0(\mathbf{r}). \tag{5}$$

The potential energy of the electron interaction with the laser field in the length gauge is

$$V_F(t) = \mathbf{r}\cdot\mathbf{F}(t). \tag{6}$$

In the Keldysh approximation, the influence of the atomic potential on the detached electron is neglected and $\Psi_{\mathbf{p}}$ is represented by the Volkov state,

$$\Psi_{\mathbf{p}}(\mathbf{r},t) = \exp\left[i(\mathbf{p}+\mathbf{k}_t)\cdot\mathbf{r} - \frac{i}{2}\int^t(\mathbf{p}+\mathbf{k}_{t'})^2dt'\right], \tag{7}$$

where $\mathbf{k}_t$ is the classical electron momentum due to the field,

$$\mathbf{k}_t = -\int^t\mathbf{F}(t')\,dt'. \tag{8}$$

It is assumed that the lower limit contribution in the integrals in Eqs. (7) and (8) is zero as if the integration is performed from $-\infty$ and the integrand is switched on adiabatically. The Volkov wave function satisfies the Schrodinger equation

$$i\frac{\partial\Psi_{\mathbf{p}}}{\partial t} = \left[-\frac{\nabla^2}{2}+V_F(t)\right]\Psi_{\mathbf{p}}. \tag{9}$$

Using Eqs. (5) and (9) and integrating by parts, we transform the amplitude in Eq. (4) into

$$A_{\mathbf{p}} = \int_0^\tau \left[E_0 - \frac{1}{2}(\mathbf{p}+\mathbf{k}_t)^2 \right] \tilde{\Phi}(\mathbf{p}+\mathbf{k}_t) \times \exp\left[\frac{i}{2}\int^t (\mathbf{p}+\mathbf{k}_{t'})^2 dt' - i E_0 t \right] dt, \quad (10)$$

where

$$\tilde{\Phi}(\mathbf{q}) = \int e^{-i\mathbf{q}\cdot\mathbf{r}} \Phi_0(\mathbf{r})\, d\mathbf{r} \quad (11)$$

is the Fourier transform of $\Phi_0(\mathbf{r})$.

B. Saddle-point method for a few-cycle pulse

The integrand in Eq. (10) contains a rapidly ocillating exponent $\exp[if(t)]$, where

$$f(t) = \frac{1}{2}\int^t (\mathbf{p}+\mathbf{k}_{t'})^2 dt' - E_0 t. \quad (12)$$

Indeed, for multiphoton processes this phase is large: $f(\tau) \sim 2\pi N|E_0|/\omega$, where $|E_0|/\omega$ is the minimum number of quanta required for photodetachment. Hence, the integral over time in Eq. (10) can be evaluated using the saddle-point method (see, e.g., Ref. [2]).

The saddle points in t are the stationary points of the phase, $f'(t) = 0$. They are roots of the equation

$$(\mathbf{p}+\mathbf{k}_t)^2 + \kappa^2 = 0, \quad (13)$$

where κ is related to the bound-state energy by $E_0 \equiv -\kappa^2/2$. Equation (13) is the classical energy conservation condition for the energies of the bound and continuum electrons. It cannot be satisfied for any real t, hence, the saddle points lie in the complex plane of time.

A crucial point in the application of the saddle-point method is that Eq. (13) corresponds to the poles of the Fourier transform $\tilde{\Phi}(\mathbf{p}+\mathbf{k}_t)$ [2]. Its behavior near the poles is, in turn, determined by the asymptotic form of the bound-state wave function at large distances,

$$\Phi_0(\mathbf{r}) \simeq B r^{\nu-1} e^{-\kappa r} Y_{lm}(\theta,\phi), \quad (14)$$

where $\nu = Z/\kappa$, Z is the charge of the atomic residue, Y_{lm} is a spherical harmonic, and B is an asymptotic normalization constant. This is an important advantage of using the length gauge [2].

For the particular case of the hydrogen negative ion ($\nu = 0$), Eqs. (11) and (14) yield

$$\tilde{\Phi}(\mathbf{p}+\mathbf{k}_t) \simeq \frac{\sqrt{4\pi}B}{(\mathbf{p}+\mathbf{k}_t)^2+\kappa^2}. \quad (15)$$

Using this and evaluating the transition amplitude (10) by the the saddle-point method, one obtains

$$A_{\mathbf{p}} = -\sum_\mu \frac{\pi\sqrt{2}B}{\sqrt{-if''(t_\mu)}} \exp[if(t_\mu)], \quad (16)$$

where the sum is over all saddle points t_μ, i.e., all complex roots of Eq. (13) in the upper half-plane of complex t. (This latter restriction is a general feature in the theory of adiabatic transitions [17].)

For a laser pulse with a sine-squared envelope, Eq. (13) takes the form

$$\left[\mathbf{p} + \frac{\mathbf{F}}{\omega} \sin^2\left(\frac{\omega t}{2N}\right) \sin(\omega t + \alpha) \right]^2 + \kappa^2 = 0. \quad (17)$$

Using $\phi = \omega t$ instead of t, one obtains the saddle-point equation as

$$p^2 + \frac{2pF\cos\theta}{\omega} \sin^2\left(\frac{\phi}{2N}\right) \sin(\phi+\alpha) + \frac{F^2}{\omega^2} \sin^4\left(\frac{\phi}{2N}\right) \sin^2(\phi+\alpha) + \kappa^2 = 0, \quad (18)$$

where θ is the angle between the photoelectron momentum $\mathbf{p}$ and the field $\mathbf{F}$.

For a long (i.e., periodic) linearly polarized laser pulse, the roots of the saddle-point equation can be found analytically [2]. It yields two pairs of complex-conjugate roots per period, two of which are in the upper half of the complex plane. The transition amplitude is then found by adding the contributions of these two saddle points. Physically, the two saddle points describe complex moments of time corresponding to the maximum electric field strength.

For the short sine-squared pulse, the saddle-point equation is solved numerically. In Sec. III, we show that numerical solution of Eq. (18) reveals $2(N+1)$ complex saddle points. They represent the "instants" in complex time at which the emission of photoelectrons takes place. We note again that the roots of the saddle-point equation are complex because ionization is a classically forbidden process, except in the case of the over-barrier regime (i.e., very strong fields). The amplitude is then given by the sum of $2(N+1)$ contributions of these saddle points, Eq. (16). This differs from the periodic pulse discussed in Ref. [2], where the amplitude was given by the contribution of only two saddle points that occur within one period. This suggests that for the N-cycle pulse, one should expect $2N$ saddle points. However, the Fourier spectrum of the field in Eq. (2) combines components with frequencies $\frac{(N+1)\omega}{N}$ and $\frac{(N-1)\omega}{N}$, which adds two more saddle points.

Explicit expressions for $f(t)$ and $f''(t)$ for the sine-squared laser pulse are given in Appendix.

III. NUMERICAL RESULTS AND DISCUSSION

In this section, we apply the formulas obtained within the adiabatic theory to consider the photodetachment of H^-. To apply our theory to H^-, we require numerical values for the asymptotic parameters B and κ of the corresponding initial bound-state wave functions. The value of B is taken from Ref. [18]. The value of κ are calculated from the corresponding binding energy as $\kappa = \sqrt{(2|E_0|)}$ using Ref. [19]. In our calculations, we have assumed a laser pulse with $N = 5$ optical cycles. We consider pulses with three peak intensities of 10^{10}, 5×10^{10}, and 10^{11} W/cm^2, with carrier-envelope phases of $\alpha = 0$, $\pi/4$, and $\pi/2$, respectively. The saddle points in each case are initially obtained by considering the 3D surface plots of $|f'(\phi)|^{-1/2}$, so that the roots of the saddle-point Eq. (13) are visualized as "infinities" rather than "zeros." The surface plots for each of the three intensities and each of the phases α reveal 12 saddle points, i.e., 12 approximate graphical solutions of the

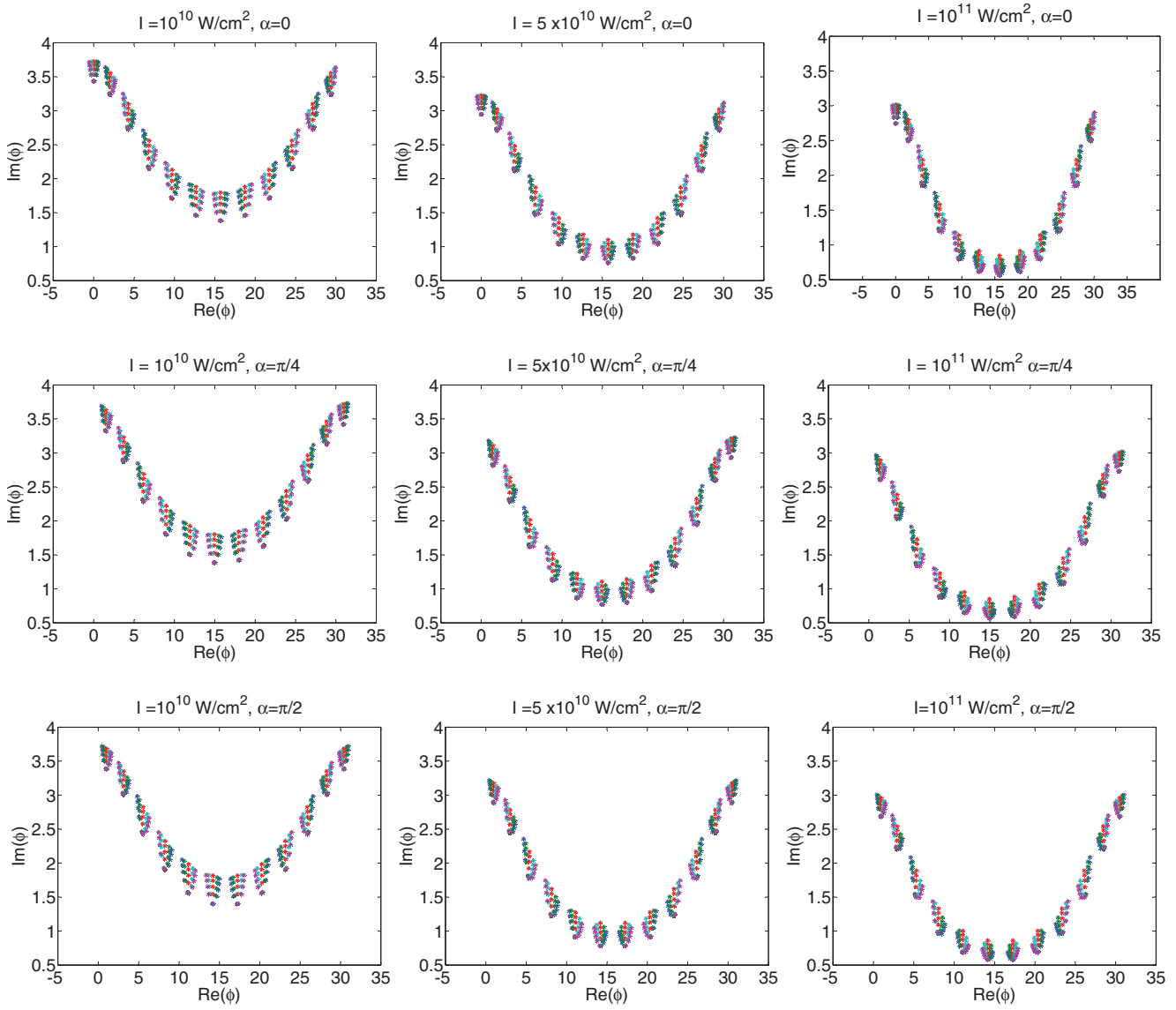

FIG. 1. (Color online) Complex-time saddle points for the 5-cycle pulse. The panels in each row represent the intensities of 10^{10}, 5×10^{10}, and 10^{11}W/cm^2. The panels in each column correspond to the CEP $\alpha = 0$, $\pi/4$, and $\pi/2$. Each group of points represent the positions of a saddle point for a range of photoelectron energies from $\varepsilon = 0.05\omega$ to $\varepsilon = 10\omega$ and angles $\theta = 0$, 45, 90, 135, and 180 degrees. In each group, the points closest to the real axis correspond to the smallest photoelectron energy.

saddle-point equation. Thus, we note that for our $N = 5$-cycle pulse, we obtain $2(N + 1)$ saddle points. This result is in agreement with Ref. [13].

The approximate roots found from the graphical solution can be improved to yield accurate values by using the Newton Raphson method for complex roots. The numerical calculation involves refining each root in turn, for a range of the angles θ between the direction of the laser field and the momentum $\mathbf{p}$ of the detached electron. In the present calculations, we consider $0 \leqslant \theta \leqslant 180^\circ$ taking a stepsize of 1°. The range of photoelectron momenta is determined by the maximum photoelectron energy taken to be 10ω. Our calculations model detachment in a 10.6-μm CO_2 laser pulse, which corresponds to the frequency $\omega = 0.0043$ a.u. The momentum values p ranging from threshold to 0.29 a.u. are obtained by considering $p = \sqrt{2\varepsilon}$ for equally spaced energies $\varepsilon_j = (\omega/20)j$ with $j = 1, 2, \ldots, 200$.

A. Saddle point "smiles"

Figure 1 illustrates the 12 roots of the saddle-point Eq. (13) for three field intensities $I = 10^{10}$, 5×10^{10}, and 10^{11} W/cm^2 and phases $\alpha = 0$, $\pi/4$, and $\pi/2$. Each "cluster" of stars in each of the nine panels in Fig. 1 shows the saddle points for five angles $\theta = 0$, 45, 90, 135, and 180 degrees (represented by different colors) and five energies in the range between $\varepsilon = 0.05\omega$ and 10ω. The change in the angle θ moves the roots mostly along the real axis, while the increase in the photoelectron energy shifts them away from the real axis. In the first row of Fig. 1, the saddle points for each of the three intensities have been calculated with the phase $\alpha = 0$, in the second row with $\alpha = \pi/4$, and in the third row with $\alpha = \pi/2$.

For each intensity and phase, the clusters of saddle points are distributed in the shape of a "smile" with the first cluster of stars on the left-hand side of each "smile" corresponding the

1st root and the last cluster on the right-hand side being the 12th root. The 12 saddle points in the complex plane of t correspond to the 12 instants at which electron detachment takes place. In each of the three rows of Fig. 1, we see that as the intensity of the laser field increases toward the center of the pulse, the saddle points move closer to the real axis. Additional calculations carried out to make a comparison with the long laser pulse considered in Ref. [2] (not shown here) depict a similiar behavior of the saddle points with laser field intensity. One can see that for each of the intensities, the increase in the pulse CEP makes the roots move along the "smile." Figure 1 also shows that the saddle points move away from the real axis with the increasing photoelectron momentum. This indicates it is more difficult for the laser pulse to kick out the electron at higher momentum.

Having found the saddle points for the laser pulse of $N = 5$ optical cycles, we obtain the transition amplitude from Eq. (16) by adding the contributions of all 12 saddle points.

B. Contribution of different saddle points to the detachment probability

In this section, we use the photodetachment amplitude to calculate the photoelectron differential detachment probability,

$$\frac{dw}{d\varepsilon d\Omega} = \frac{2p|A_{\mathbf{p}}|^2}{(2\pi)^3}, \tag{19}$$

where the factor of 2 accounts for the two electrons in the hydrogen negative ion. We also calculate the photoelectron energy spectrum,

$$\frac{dw}{d\varepsilon} = 2\pi \int_0^{\pi} \frac{dw}{d\varepsilon d\Omega} \sin\theta d\theta, \tag{20}$$

and total detachment probability,

$$w = \int_0^{\infty} \frac{dw}{d\varepsilon} d\varepsilon. \tag{21}$$

The differential probability in Eq. (19) is similar to the differential detachment *rate*, which characterizes the process for a long periodic laser pulse [2]. However, for the long pulse, the photoelectron spectrum consists of a set of discrete δ-function spikes corresponding to the n-photon absorption, with energies $\varepsilon_n = n\omega - |E_0| - F^2/4\omega^2$ (where the last term is the ponderomotive shift). In contrast, in the short pulse the photoelectron energy distribution is continuous, with the n-photon processes manifesting themselves as broad peaks centered at $\varepsilon \approx n\omega - |E_0|$.

Physically, the process of multiphoton electron detachment can be understood as tunneling in the slowly varying external potential [2] (hence, the adiabatic treatment used in Sec. II). For a short pulse, this means that the electron detachment should occur mostly near the maximum of the pulse where the electric field is strongest. One can then expect that in the saddle-point treatment of the transition amplitude, the saddle points closest to the center of the pulse will give the largest contribution to the sum in Eq. (16).

Each row in Fig. 2 shows the differential detachment probabilities obtained by including different numbers of the saddle points in the transition amplitude. The three rows correspond to the peak intensities of 10^{10}, 5×10^{10}, and 10^{11} W/cm^2, respectively. Each panel depicts a range of θ and photoelectron energies ε for the CEP $\alpha = 0$. Considering the first row of Fig. 2 with the lowest intensity $I = 10^{10}$ W/cm^2, it is clear that there is a very small probability that the electron will be detached with a high energy. This may be noted from the large flat area in each of the panels of row one. Next, considering rows two and three, we see that the probability of electron detachment with a higher energy increases with increasing field intensity. This result illustrates the fact that at higher intensities it is easier for the electron to absorb more excess photons from the laser pulse.

By comparing the first panel in each row with the second panel, we note that the main contribution to total detachment probability comes from the middle five saddle points, i.e., saddle points 5–9. Thus, we see that neglecting the contributions of the seven outer saddle points (i.e., 1–4, located on the left-hand side of the "smiles" shown in Fig. 1, and 10–12, located on the right-hand side of the "smiles") does not affect the magnitude of the detachment probability. This result is true for each of the intensities considered.

By comparing the second panel in each row, the second with the third panel, we see that the middle *three* saddle points (6–8) make a dominant contribution to the detachment probability. These are the saddle points closest to the real axis. However, there are noticeable deviations in the oscillatory structures between the panels in the second and third columns. This means that the interference effects due to the contributions of different saddle points to the amplitude Eq. (16) are sensitive to the contributions of the saddle points 5 and 9.

Table I shows the total detachment probabilities obtained by including various saddle-point contributions for $\alpha = 0$ and the three peak intensities. For $I = 10^{10}$ W/cm^2, it may be seen that the contributions from the middle five saddle points (5–9) gives a 99.67% contribution to the detachment probability. We observe that the contribution from the 3 central saddle points (6–8) gives a slightly larger detachment probability than the contribution from the 5 middle saddle points (or all 12 saddle points). This suggests that there are some interference effects at this intensity and phase corresponding to coherent detachment of electrons at different instants of time. In the case of $I = 5 \times 10^{10}$ W/cm^2, it is observed that the five saddle points (5–9) give a 99.96% contribution to the final detachment probability. The three central saddle points yield a 95.44% contribution to the total detachment probability. We also note that there is no interference effect at this intensity. Finally, in the case of $I = 10^{11}$ W/cm^2, the 5 central roots give a 99.92% contribution to the total detachment probability and the three roots closest to the real axis give a 92% contribution to the total detachment probability.

These results confirm our graphical results that it is the saddle points closest to the real axis that contribute most to the detachment amplitude. Our calculations suggest the crude result that for an N-cycle pulse, the N middle saddle points closest to the real axis will yield the near total probability of detachment at the lower intensity of 10^{10} W/cm^2 and the total detachment probability at the higher intensity of 5×10^{10} W/cm^2 and above. Furthermore, our results in this section also show that the adiabatic theory for the short laser pulse predicts the oscillatory nature of the detachment probabilities

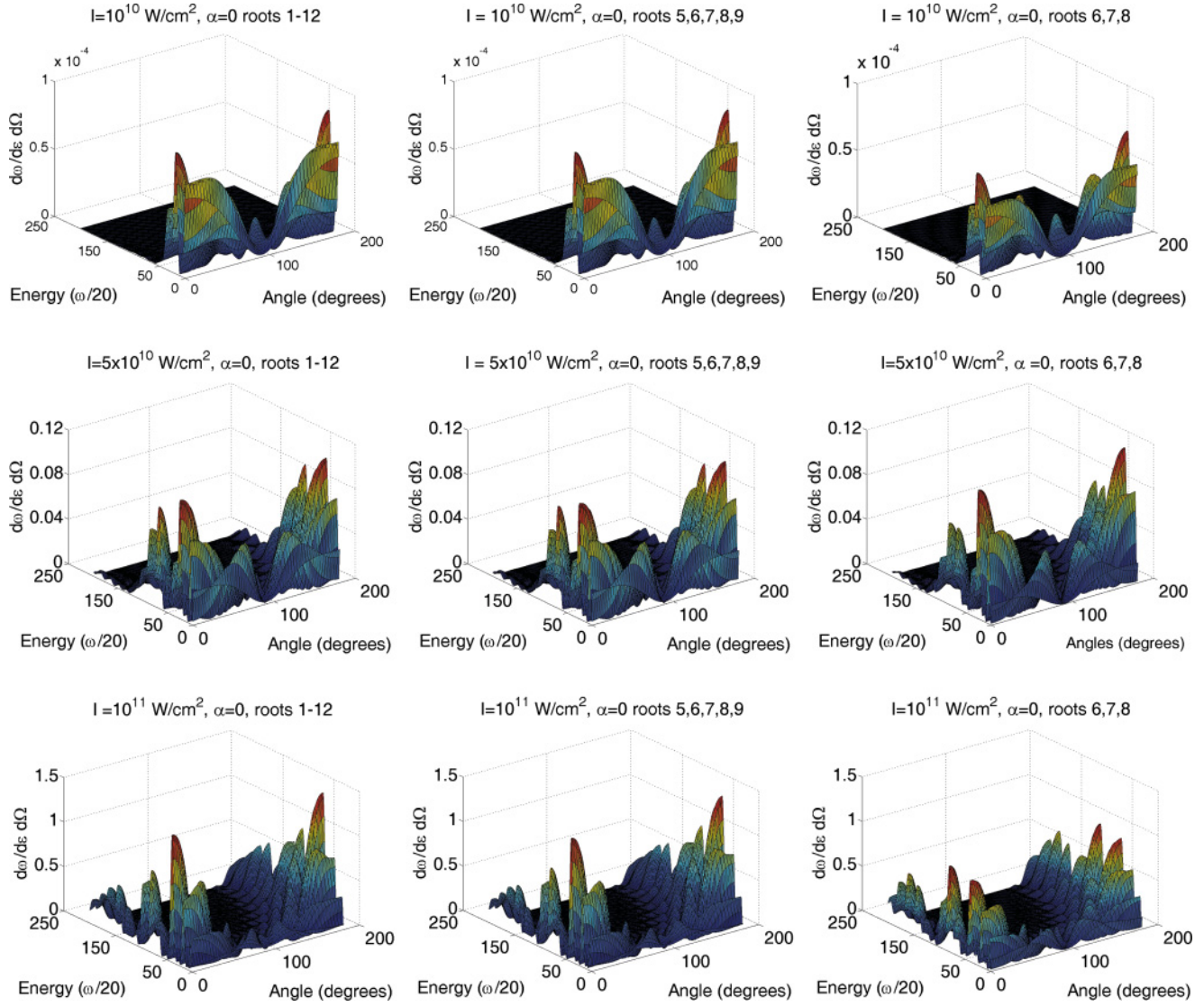

FIG. 2. (Color online) Differential detachment probabilities $d\omega/d\varepsilon d\Omega$ for CEP $\alpha = 0$. In each row, the first panel shows the detachment probability calculated using all 12 saddle points, the second panel shows the contribution of the central 5 saddle points (5–9), and the third panel shows the contribution of the middle 3 saddle points (6–8). The first row is for the peak intensity of $I = 10^{10}$, second for 5×10^{10}, and third for 10^{11} W/cm^2. The energy axis in each plot shows the photoelectron energy in units of $\omega/20$.

as a result of interference caused by the electrons detached at different instants of time.

Let us now turn to the effect of the carrier-envelope phase on the detachment probability. Figure 3 shows the differential detachment probabilities calculated using all 12 saddle points

TABLE I. Total detachment probabilities from H^- by 5-cycle pulses with the CO_2 laser frequency $\omega = 0.0043$ for CEP $\alpha = 0$. The total detachment probabilities are calculated considering the contribution from all 12, the central 5 (5–9), and the inner 3 (6–8) saddle points.

	Intensity		
Roots	10^{10} W/cm^2	5×10^{10} W/cm^2	10^{11} W/cm^2
1–12	1.496×10^{-6}	2.568×10^{-3}	2.574×10^{-2}
5–9	1.491×10^{-6}	2.567×10^{-3}	2.572×10^{-2}
6–8	1.500×10^{-6}	2.451×10^{-3}	2.368×10^{-2}

for the three sets of intensities and three phases: $\alpha = 0$, $\pi/4$, and $\pi/2$. For the intensity of 10^{10} W/cm^2, we see that changing the phase has little effect on the detachment probabilitity. It is

TABLE II. Total detachment probabilities from H^- by 5-cycle pulses with the CO_2 laser frequency $\omega = 0.0043$ for different intensities and carrier-envelope phases.

Phase	Intensity		
α	10^{10} W/cm^2	5×10^{10} W/cm^2	10^{11} W/cm^2
0	1.496×10^{-6}	2.568×10^{-3}	2.574×10^{-2}
$\pi/4$	1.492×10^{-6}	2.514×10^{-3}	2.549×10^{-2}
$\pi/2$	1.488×10^{-6}	2.523×10^{-3}	2.585×10^{-2}
GK[a]	1.32×10^{-6}	2.57×10^{-3}	2.24×10^{-2}

[a]GK is the detachment probability estimated by multiplying the detachment rate for the periodic pulse from Ref. [2] by the effective 5-cycle pulse duration chosen to be $T = 2\pi/\omega$.

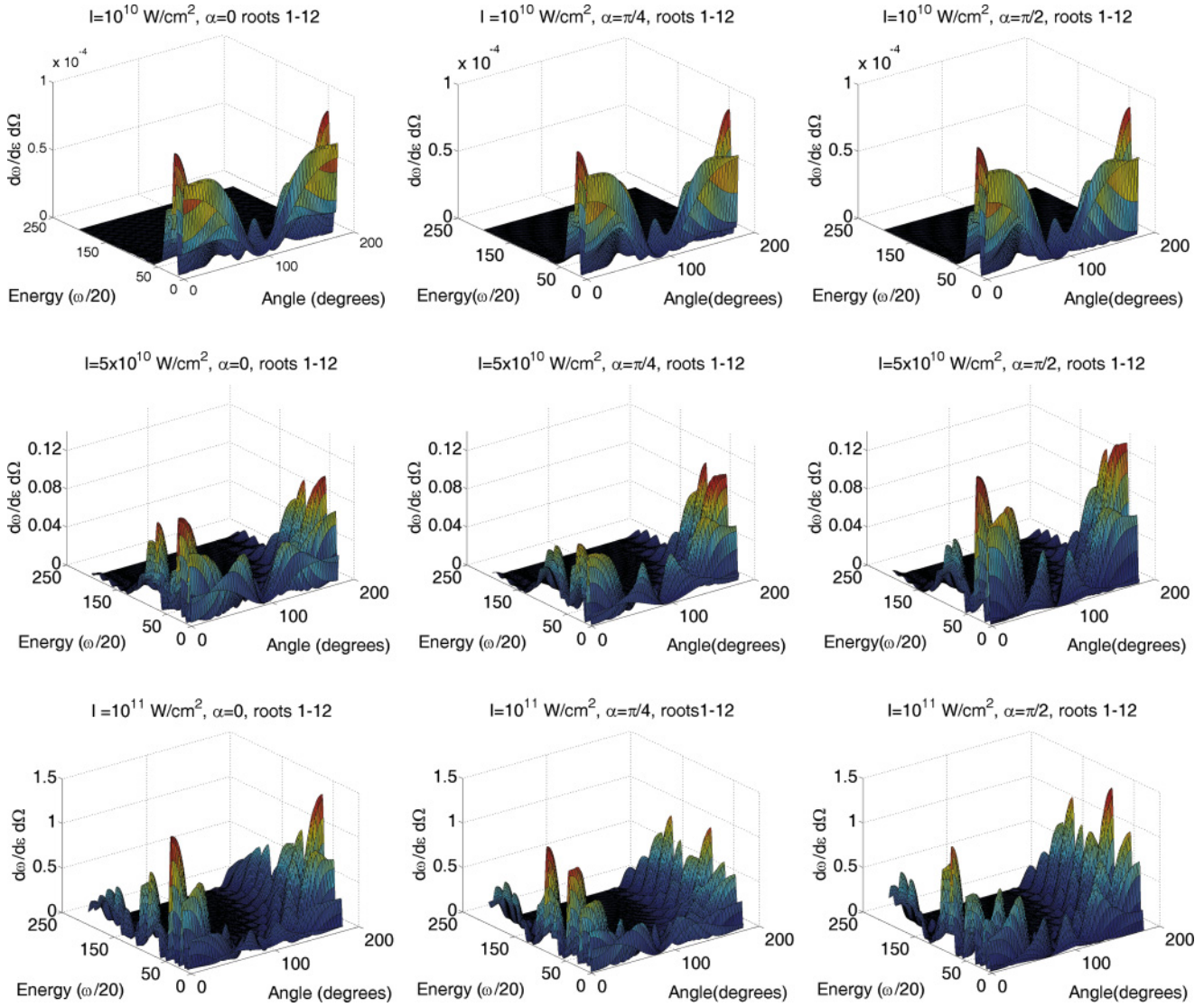

FIG. 3. (Color online) Differential detachment probabilities $d\omega/d\varepsilon d\Omega$ for different CEP values, $\alpha = 0$, $\pi/4$, and $\alpha = \pi/2$ (columns one to three, respectively), and different peak intensities, $I = 10^{10}$, 5×10^{10}, and $10^{11}\mathrm{W/cm^2}$ (rows one to three, respectively). The energy axis shows the photoelectron energy in units of $\omega/20$.

also observed from Fig. 3 that for the higher intensities of 5×10^{10} and 10^{11} W/cm^2 (rows two and three, respectively), the increase in the phase makes the angular distributions markedly asymmetric. Thus, the CEP has an important influence on the photoelectron probability distributions. Another pattern that is observed in all the panels in Fig. 3 is that as the intensity

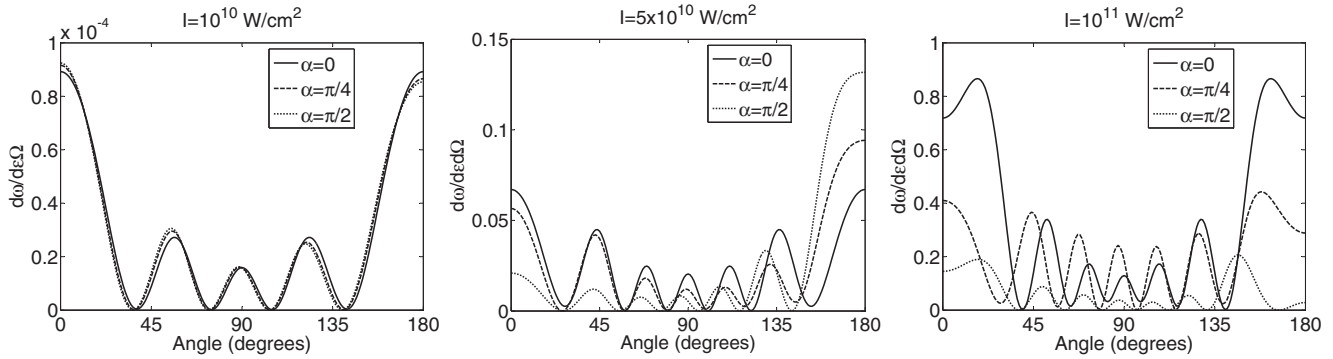

FIG. 4. Dependence of the photoelectron angular distribution on the carrier-envelope phase α for the three intensities, $I = 10^{10}$ (panel 1), 5×10^{10} (panel 2), and 10^{11} W/cm^2 (panel 3). For each intensity, the photoelectron energy corresponds to a maximum in the electron energy spectrum, $\varepsilon = \omega$ (10^{10} and 10^{11} W/cm^2), and $\varepsilon = 1.25\omega$ (5×10^{10} W/cm^2).

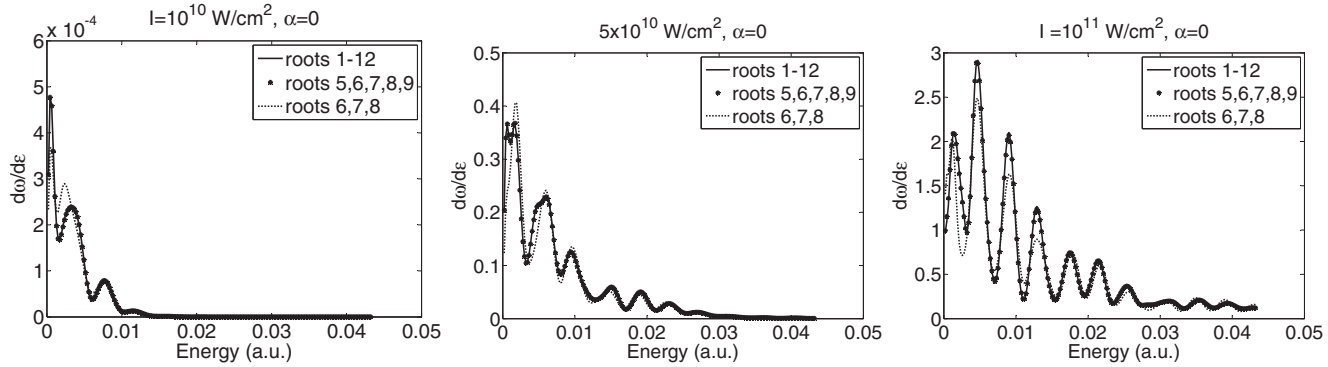

FIG. 5. Photoelectron energy spectra calculated for the CEP $\alpha = 0$ by including a different number of saddle points in the amplitude: 3 (6–8), shown by dotted line; 5 (5–9), shown by asterisks; and all 12 (dashed line). The peak intensities are 10^{10} W/cm^2 (panel 1), 5×10^{10}W/cm^2 (panel 2), and 10^{11} W/cm^2 (panel 3).

increases, the probability of detachment also increases. These results are confirmed in Table II.

Table II shows the total detachment probabilities for H^- in the 5-cycle pulse for the three peak intensities and three CEP values: $\alpha = 0$, $\pi/4$, and $\pi/2$. From the table, two trends are observed. The first is that, as expected, the larger peak intensities result in greater detachment probabilities. The second trend shows that the numerical values of the detachment probabilities do not have a strong dependence on the CEP for all intensities considered. In order to check our detachment probabilities in Table II, we compared our results with the detachment rates of the periodic pulse obtained in Table I of Ref. [2]. The effective pulse length for a 5-cycle short laser pulse is about one period, i.e., $2\pi/\omega$. Thus, to make the comparison between the two sets of results, we took the total detachment rates from Table I of Ref. [2] and multiplied this sum by the period of the pulse. Our present results are in excellent agreement with the long pulse calculations in Ref. [2].

C. Angular dependence on carrier-envelope phase

The dependence of the photoelectron angular distribution on the CEP is examined in Fig. 4. Here, slices of the 3D graphs from Fig. 3 were taken, with all 12 saddle points included in the evaluation of the transition amplitude. For each intensity, the photoelectron energy was chosen to correspond with the most likely probability of detachment (see Sec. III D), and the detachment probability was plotted against θ.

From the graphs, it is evident that at the lowest intensity varying the CEP has very little effect on the detachment probability. Here the detachment energy is $\varepsilon = \omega$. The distributions in panel 1 of Fig. 4 are notably symmetric for all phases considered. In the second panel of Fig. 4, we see that as the intensity is increased to 5×10^{10} W/cm^2, the CEP has a more marked effect on the magnitude of the detachment probability. Here, the detachment energy is $\varepsilon = 1.25\omega$. In this case, the angular distribution is symmetric for $\alpha = 0$ but becomes increasingly asymmetric as the phase is increased. In the third case in which $I = 10^{11}$ W/cm^2 with the detachment energy $\varepsilon\omega$, we note that $\alpha = 0$ again yields a symmetric angular distribution, but again as the phase shift increases the angular distributions become asymmetric. We also observe from Fig. 4 that the detachment probability is increased with increasing intensity.

D. Energy spectrum

Here, we consider the photoelectron energy spectrum that is given by Eq. (20). The energy spectra are shown in Figs. 5 and 6. The most noticeable feature of the spectra is the presence of peaks spaced by $\Delta\varepsilon \approx \omega$. Each of these "above-threshold" peaks results from the ejection of the electron following the absorption of a different number

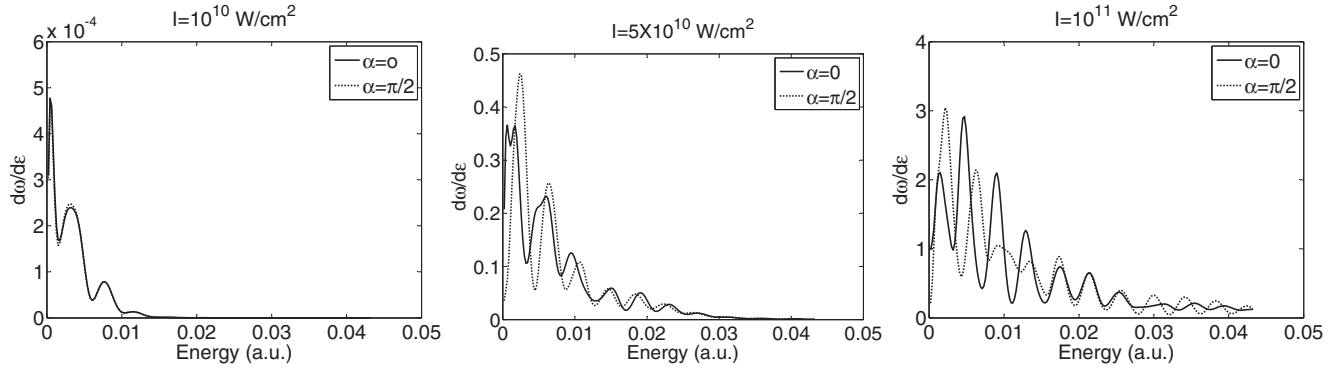

FIG. 6. Photoelectron energy spectra calculated using all 12 saddle points for the CEP α=0 (solid line) and $\alpha = \pi/2$ (dashed line) and three peak intensities: 10^{10} W/cm^2 (panel 1), 5×10^{10}W/cm^2 (panel 2), and 10^{11} W/cm^2 (panel 3).

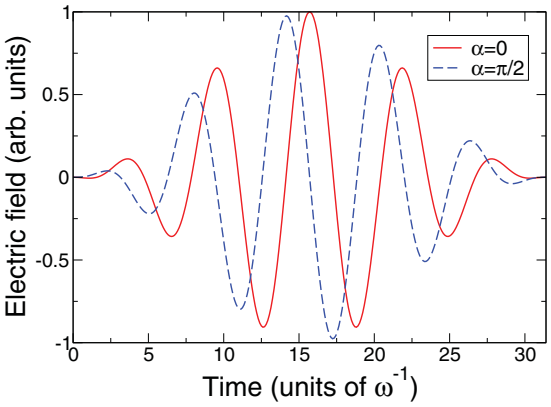

FIG. 7. (Color online) Electric field in the short pulse with the CEP $\alpha = 0$ (solid red line) and $\pi/2$ (dashed blue line).

of photons. Since the photons in the short pulse are not mono-energetic (that is, their energies have an uncertainty $\Delta\omega \sim 2\pi/\tau = \omega/N$), the peaks are broadened in comparison with the above-threshold peaks that one would observe with a long pulse (see, e.g., Table I in Ref. [2], which illustrates the detachment probability for the absorption of n monoenergetic photons).

In Fig. 5 we show how the behavior of the spectrum is affected by the number of saddle points considered within the transition amplitude. It can be seen from all three graphs that it is the central five saddle points (5–9) that dominate the behavior of the energy spectra for all three intensities considered. The calculation that includes only three central saddle points (6–8) shows significant deviations from the five-saddle-point calculation. This confirms our earlier results from the 3D surface plots considered in Fig. 3. The graphs also show that the spectra obtained with 5 saddle points are almost indistinguishable from the results obtained with all 12 saddle points.

In Fig. 6, we analyze the dependence of the electron energy spectra on the CEP. It appears that $\alpha = \pi/2$ gives rise to higher maximum values of the spectra. In order to understand this dependence of the photoelectron energy spectrum on the phase, it is useful to look at the profile of the electric field for different carrier-envelope phases. The field is given by Eqs. (1) and (2), and we illustrate the field for the two cases of $\alpha = 0$ and $\alpha = \pi/2$ in Fig. 7.

From Fig. 7, it may be seen that for $\alpha = 0$ the field reaches its maximum strength, once maximal in the middle of the pulse. On the other hand, for $\alpha = \pi/2$, the electric field has a maximum and minimum of equal absolute value near the middle of the pulse. Hence, the larger detachment probability for $\alpha = \pi/2$ may be related to the fact that, in this case, the electric field strength takes its largest value twice near the center of the pulse, and that its maximum magnitude is only slightly lower than the single peak value for $\alpha = 0$.

IV. CONCLUSIONS

In conclusion, we have extended the adiabatic method of Ref. [2] to describe electron detachment from negative ions in a short laser pulse. In this approach we have found that a linearly polarized pulse with N cycles results in $2(N + 1)$ saddle points in complex time, which contribute to the transition amplitude. Our calculations show that the N inner saddle points, i.e., those closest to the pulse maximum, dominate the behavior of the transition amplitude. The detachment probabilities show three main features. First, they have a strong dependence on the dominant saddle point contributions; second, they are highly asymmetric; and third, their magnitude is independent of the CEP. It should be noted here that the envelope of the pulse is chosen to be sine-squared for convenience. Other pulse envelopes such as the Gaussian envelope adopted in Ref. [14] should yield a similar effect to the present calculations.

Our calculations predict an interference structure and a phase dependence in both the photoelectron angular distributions and energy spectra. In particular, we can identify the actual saddle points that cause the interference structures due to the electrons emitted at various complex moments of time. The dependence of the electron angular distribution on the carrier-envelope phase provides a new method for measuring the absolute phase of the pulse.

Finally, the findings of this work allow a simple qualitative and quantitative physical analysis of the problem of electron detachment from negative ions in a short laser pulse and may be of use to experimentalists.

APPENDIX: CLASSICAL ACTION FOR THE SINE-SQUARED PULSE

To calculate the transition amplitude Eq. (16), we need to evaluate $f(t)$ from Eq. (12) and $f''(t)$. For the sine-squared laser pulse, Eq. (2), the momentum due to the field is

$$\mathbf{k}_t = \frac{\mathbf{F}}{\omega}\sin^2\left(\frac{\phi}{2N}\right)\sin(\phi+\alpha), \tag{A1}$$

where $\phi = \omega t$. Hence, one obtains

$$\begin{aligned} f(t) = {} & \frac{1}{2}p^2 t - E_0 t - \frac{\mathbf{p}\cdot\mathbf{F}}{2\omega^2}\cos(\phi+\alpha) + \frac{\mathbf{p}\cdot\mathbf{F}}{4\omega^2}\left[\frac{N}{N+1}\cos\left(\frac{N+1}{N}\phi+\alpha\right) + \frac{N}{N-1}\cos\left(\frac{N-1}{N}\phi+\alpha\right)\right] \\ & + \frac{3F^2 t}{32\omega^2} - \frac{F^2 N}{8\omega^3}\sin\frac{\phi}{N} + \frac{F^2 N}{64\omega^3}\sin\frac{2\phi}{N} - \frac{3F^2}{64\omega^3}\sin(2\phi+2\alpha) + \frac{F^2}{16\omega^3}\left[\frac{N}{1-2N}\sin\left(\frac{1-2N}{N}\phi-2\alpha\right)\right. \\ & \left. + \frac{N}{1+2N}\sin\left(\frac{1+2N}{N}\phi+2\alpha\right)\right] - \frac{F^2}{128\omega^3}\left[\frac{N}{1-N}\sin\left(\frac{2(1-N)}{N}\phi-2\alpha\right) + \frac{N}{1+N}\sin\left(\frac{2(1+N)}{N}\phi+2\alpha\right)\right], \end{aligned} \tag{A2}$$

and

$$f''(t) = \frac{\mathbf{p}\cdot\mathbf{F}}{2N}\sin\frac{\phi}{N}\sin(\phi+\alpha) + \mathbf{p}\cdot\mathbf{F}\sin^2\frac{\phi}{2N}\cos(\phi+\alpha) + \frac{F^2}{2\omega N}\sin\frac{\phi}{N}\sin^2\frac{\phi}{2N}\sin^2(\phi+\alpha) + \frac{F^2}{\omega}\sin^4\frac{\phi}{2N}\cos(\phi+\alpha)\sin(\phi+\alpha). \quad \text{(A3)}$$

[1] P. B. Corkum and F. Krausz, Nature Phys. **3**, 381 (2007).
[2] G. F. Gribakin and M. Yu. Kuchiev, Phys. Rev. A **55**, 3760 (1997).
[3] L. V. Keldysh, Zh. Eksp. Teor. Fiz. **47**, 1945 (1964) [Sov. Phys. JETP **20**, 1307 (1965)].
[4] M. Yu. Kuchiev and V. N. Ostrovsky, Phys. Rev. A **59**, 2844 (1999).
[5] R. Reichle, H. Helm, and I. Yu. Kiyan, Phys. Rev. Lett. **87**, 243001 (2001).
[6] I. Yu. Kiyan and H. Helm, Phys. Rev. Lett. **90**, 183001 (2003).
[7] H. R. Reiss, Phys. Rev. A **77**, 067401 (2008).
[8] B. Bergues, Z. Ansari, D. Hanstorp and I. Yu. Kiyan, Phys. Rev. A **77**, 067402 (2008).
[9] B. Bergues, Z. Ansari, D. Hanstorp and I. Yu. Kiyan, Phys. Rev. A **75**, 063415 (2007).
[10] T. K. Kjeldsen and L. B. Madsen, J. Phys. B **6**, 2033 (2004).
[11] D. Bauer, D. B. Milosevic, and W. Becker, Phys. Rev. A **72**, 023415 (2005).
[12] D. B. Milošević, G. G. Paulus, D. Bauer, and W. Becker, J. Phys. B **39**, R203 (2006).
[13] C. P. J. Martiny and L. B. Madsen, Phys. Rev. A **78**, 043404 (2008).
[14] C. Arendt, D. Dimitrovski, and J. S. Briggs, Phys. Rev. A **76**, 023423 (2007).
[15] T. P. Grozdanov and J. Jacimovic, Phys. Rev. A **79**, 013413 (2009).
[16] X. Liu and C. Figueira de Morrison Faria, Phys. Rev. Lett. **92**, 133006 (2004).
[17] L. D. Landau and E. M. Lifshitz, *Quantum Mechanics. Nonrelativistic Theory* (Peragmon, Oxford, 1965).
[18] E. E. Nikitin and B. M. Smirnov, *Atomic and Molecular Processes* (Nauka, Moscow, 1988).
[19] H. Hotop and W. C. Lineberger, J. Phys. Chem. Ref. Data **14**, 731 (1985).